Supporting Information
Symmetry-Breaking Charge Separation in Perylene Diimide Trimers: Effects of Aggregation and Solvent Polarity

Lie Tian[1,#], Guangliu Ran[1,2,#*], Shixuan Zheng[3], Wenkai Zhang[1,2*]

1 School of Physics and Astronomy, Applied Optics Beijing Area Major Laboratory, Center for Advanced Quantum Studies, Beijing Normal University, Beijing 100875, China

2 Key Laboratory of Multiscale Spin Physics, Ministry of Education, Beijing Normal University, Beijing 100875, China

3 Beijing National Laboratory for Molecular Science, State Key Laboratory of Rare Earth Materials Chemistry and Applications, College of Chemistry and Molecular Engineering, Peking University, Beijing 100871, China

AUTHOR INFORMATION

[#]These authors contribute equally to this work

Corresponding Author

*E-mail: wkzhang@bnu.edu.cn, bnurgg@bnu.edu.cn

1. Sample Preparation

The details of molecular structures, design and synthesis methods of PDI-III can be seen in the literature.[1] All the essential materials and organic solvents were bought from the certified commercial resources and used as received.

2. Experimental Methods

For solution experiments, ultraviolet-visible (UV-Vis), fluorescence and transient absorption spectra (TAS) were recorded with Agilent Technologies Cary 60 UV−visible spectrophotometer, FLS980 spectrometer (Edinburgh), and ultrafast TA spectrometer (Harpia-TA, Light Conversion), respectively. Details of the instrument have been described in a previous article.[2] The TA experiments were performed multiple times at different positions of the cell. No sample degradation was observed after the measurements, and the pump fluence was kept at 5.1 μJ cm^{-2} unless stated otherwise. The fluorescence quantum yield was measured by the comparative method.[3] Global analysis of the TAS data was performed using the Glotaran program.[4]

Time-resolved infrared (TRIR) measurements were performed as follows. A commercial Ti:Sapphire amplifier (Astrella, Coherent) operating at 1 kHz was used to pump an optical parametric amplifier with dual outputs (TOPAS-TWINS, Light Conversion). Mid-infrared probe pulses were generated from the high-energy output via difference frequency generation in $AgGaS_2$ nonlinear crystal. The low-energy output was used to generate visible light, which acted as the pump in the TRIR measurements. Time delays between the pump and probe pulses were controlled with a mechanical delay stage, and the relative polarization angles of the two pulses were

set to the magic angle. The sample was mounted on a two-dimensional translation stage, allowing horizontal and vertical movement to prevent sample damage. After transmission through the sample, the pump was blocked, and the probe was dispersed by a monochromator (SP-2150, Teledyne Princeton Instruments) and detected using a liquid nitrogen-cooled 128×128 MCT array (2DMCT, Phasetech Spectroscopy). The pump fluence was maintained at 12.7 μJ cm^{-2}.

3. Computational Methods

Conformational searches for PDI-III and its dimers in acetone were performed using the Molclus program[5] coupled with the xtb software.[6] Molecular dynamics (MD) simulations with GFN force-field (GFN-FF)[7] were conducted at 400 K to generate possible conformations. The resulting structures were subsequently optimized at the GFN0-xTB[8] level and clustered for initial screening. Representative low-energy structures from each cluster were selected for further refinement using the GFN2-xTB[9] method combined with the GBSA solvation model to account for solvent effects. Vibrational frequency analysis was performed on the global minimum structures to calculate Gibbs free energies.

For PDI-III in toluene, explicit solvent effects were taken into account. MD simulations were carried out using the GROMACS 2023 package[10] with the Generalized Amber Force Field (GAFF).[11] RESP2(0.5) charges[12] were derived using Multiwfn software[13, 14], based on wavefunctions calculated by ORCA program[15] at the B3LYP[16]/def2-TZVP[17] level, and topology files were generated via the Sobtop.[18] Simulation boxes containing either one PDI-III molecule with 500 toluene molecules

or two PDI-III molecules with 1000 toluene molecules were constructed using Packmol.[19] Following energy minimization, MD simulations were performed under the NPT ensemble. The temperature was maintained at 298.15 K using a velocity-rescale thermostat,[20] while the pressure was kept at 1 atm using a stochastic cell rescaling barostat.[21] Periodic boundary conditions (PBC) were applied with a time step of 1 fs. Electrostatic and van der Waals interactions were treated using the Particle-Mesh Ewald (PME) method[22] with a cutoff of 1.0 nm. Bond lengths involving hydrogen atoms were constrained using the LINCS algorithm.[23] Upon reaching equilibrium, snapshots were extracted every 500 ps and subjected to screening via the Molclus[5] workflow. Finally, the Gibbs free energies were evaluated using the GFN2-xTB5 method with GBSA model.

Table S1 Calculated Gibbs Free Energies of the PDI-III Monomer and Dimer in Different Solvents.

Solvent	$G_{monomer}$ (a.u.)	G_{dimer}(a.u.)	ΔG (kcal mol^{-1})
Acetone	-936.672774	-468.342087	+7.2
Toluene	-936.719693	-468.354426	-6.8

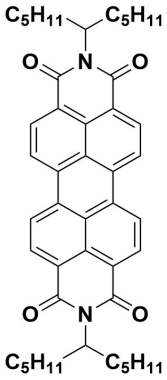

Figure S1. The reference molecular structure of PDI-C5.

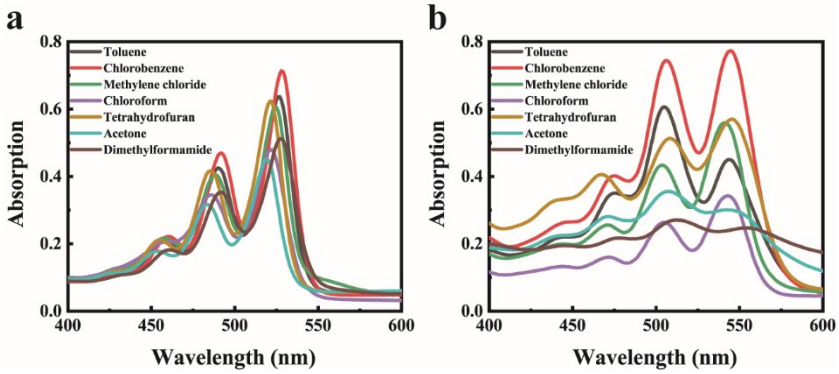

Figure S2. UV-Vis spectra at different solvents of (a) PDI-C5, and (b) PDI-III. Concentration is 10^{-5} mM/mL

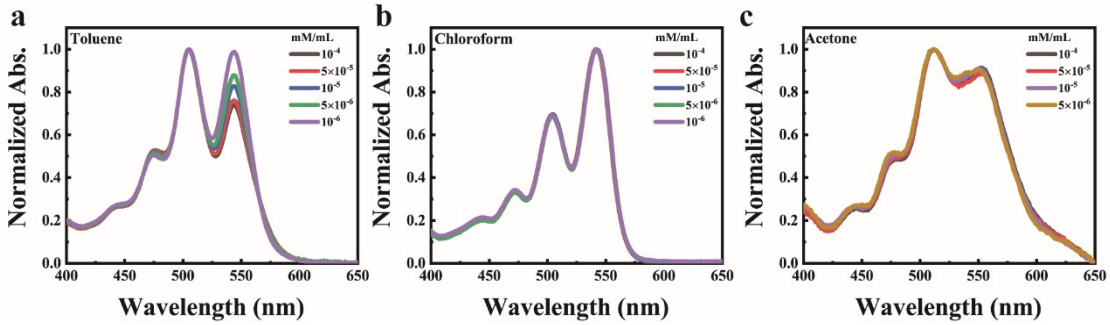

Figure S3. The normalized UV-Vis spectra of PDI-III at (a) Toluene, (b) Chloroform and (c) Acetone at different concentration.

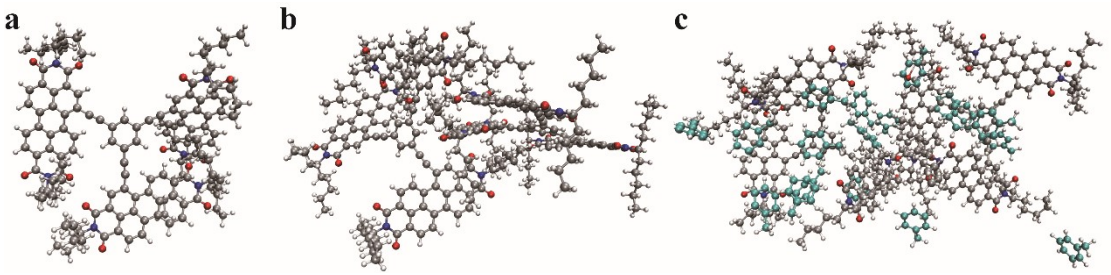

Figure S4. (a) Lowest-energy structure of a single PDI-III monomer in acetone obtained from the conformational search. (b) Lowest-energy intermolecularly aggregated structure of two PDI-III molecules in toluene derived from the conformational search. (c) Snapshot of the PDI-III dimer in toluene extracted from MD simulations, with adjacent toluene molecules explicitly displayed. Toluene molecules are shown in cyan and are observed to occupy the interstitial space between the two PDI-III units, mediating their π-π stacking interactions and stabilizing the dimeric configuration.

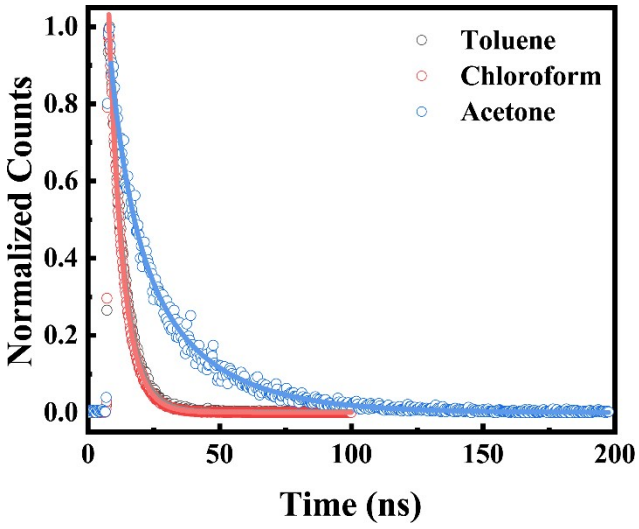

Figure S5. Normalized fluorescence lifetime decay, excited at 480 nm.

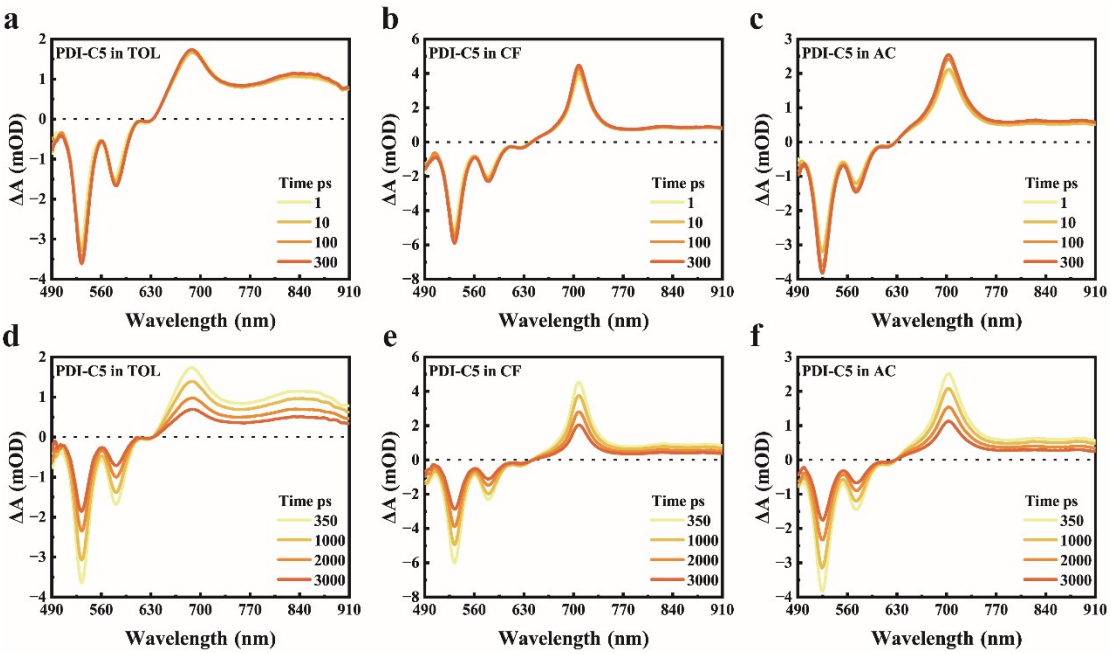

Figure S6. TAS spectra results of PDI-C5 in (a, d) toluene, (b, e) chloroform, and (c, f) acetone, recorded at short (a-c) and long (d-f) time delays following 480 nm excitation.

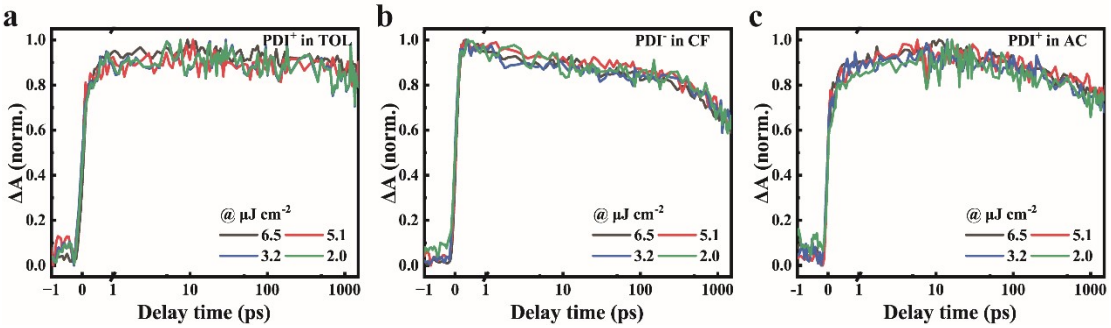

Figure S7. Normalized TAS kinetic traces in toluene (a), chloroform (b), and acetone (c) measured at different excitation fluences. The kinetic traces show excellent overlap over the entire range of pump fluences, indicating that the formation and decay dynamics are independent of the excitation density within the investigated regime.

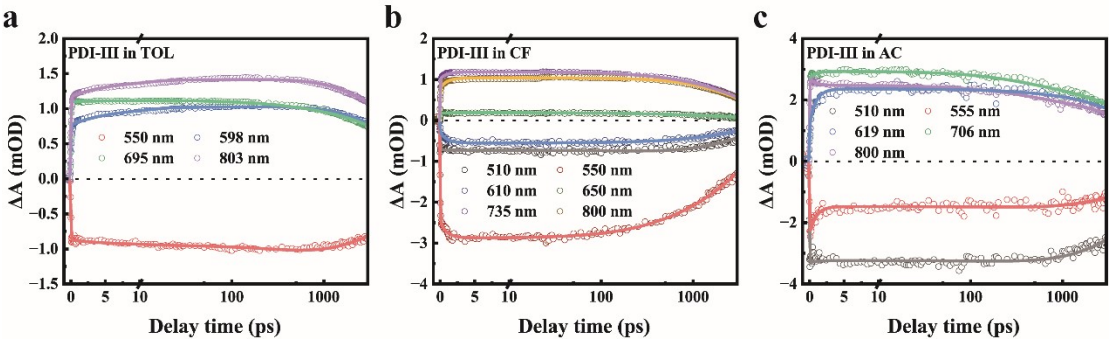

Figure S8. TAS spectra and global fitting results of PDI-III in toluene (a), chloroform (b), and acetone (c). Circles represent the experimental data, and solid lines correspond to the global fitting results.

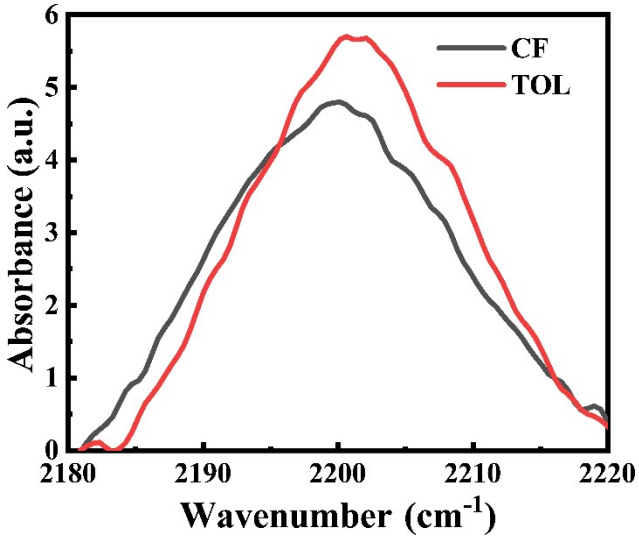

Figure S9. Fourier-transform infrared spectra (FTIR) of PDI-III in chloroform and toluene. The concentration of PDI-III in chloroform and toluene was 5 × 10^{-3} mM/mL, while its FTIR spectrum in acetone could not be measured due to low solubility. For the TRIR experiment in acetone, a saturated solution of PDI-III was used.

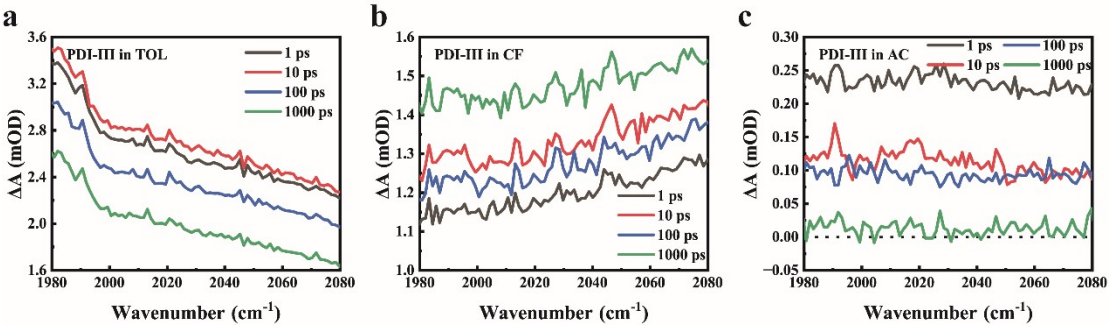

Figure S10. TRIR spectra of PDI-III in toluene (a), chloroform (b), and acetone (c) around 2050 cm^{-1} region following 480 nm excitation.

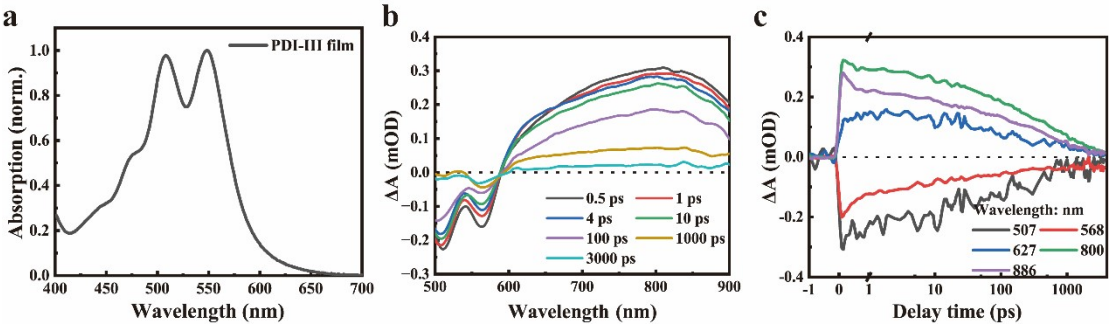

Figure S11. (a) UV-Vis absorption spectrum of a PDI-III film. (b) TAS spectra recorded at selected delay times following 480 nm excitation. An isosbestic point appears at approximately 660 nm as the delay time increases to 4 ps, accompanied by the decay of the excited-state absorption band around 780 nm and the concomitant growth of a new absorption band at ~620 nm. (c) Corresponding kinetic traces monitored at the indicated wavelengths.

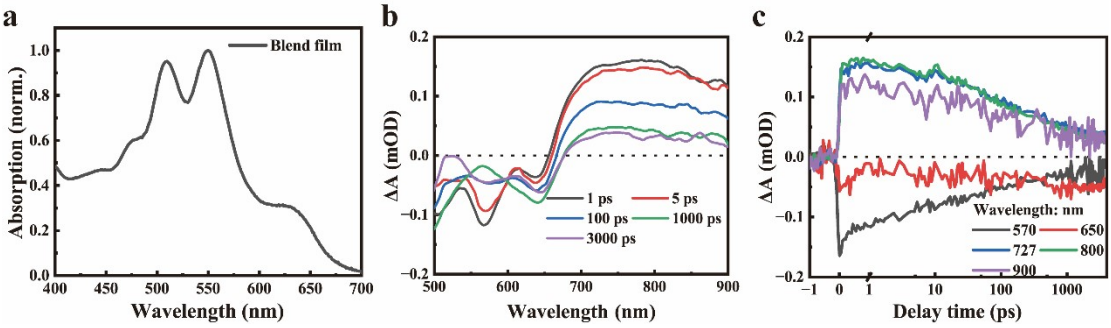

Figure S12. (a) UV-Vis absorption spectrum of a PBDB-T:PDI-III blend film. (b) TAS spectra recorded at selected delay times following 480 nm excitation. The GSB at ~570 nm is assigned to PDI-III, whereas the GSB at ~650 nm originates from PBDB-T. (c) Corresponding kinetic traces monitored at the indicated wavelengths. Upon 480 nm excitation, PBDB-T is directly excited, leading to a rapid increase of the donor GSB at early delay times followed by its decay, while the subsequent growth of the donor GSB at longer delay times is attributed to charge separation from the PDI-III (~650 nm).

Supporting References:

1. H. Wang, M. Li, Y. Liu, J. Song, C. Li and Z. Bo, *J. Mater. Chem. C*, 2019, **7**, 819-825.
2. G. Ran, J. Zeb, H. Lu, Y. Liu, A. Zhang, L. Wang, Z. Bo and W. Zhang, *J.Phys. Chem. Lett.*, 2022, **13**, 5860-5866.
3. A. T. R. Williams, S. A. Winfield and J. N. Miller, *Analyst*, 1983, **108**, 1067-1071.
4. J. J. Snellenburg, S. Laptenok, R. Seger, K. M. Mullen and I. H. M. van Stokkum, *J. Stat. Softw.*, 2012, **49**, 1 - 22.
5. T. Lu, Molclus, Version 1.13, http://www.keinsci.com/research/molclus.html (accessed 2026-02-27).

6. C. Bannwarth, E. Caldeweyher, S. Ehlert, A. Hansen, P. Pracht, J. Seibert, S. Spicher and S. Grimme, *WIREs Comput. Mol. Sci.*, 2021, **11**, e1493.
7. S. Spicher and S. Grimme, *Angew. Chem. Int. Ed.*, 2020, **59**, 15665-15673.
8. P. Pracht, E. Caldeweyher, S. Ehlert and S. Grimme, *ChemRxiv*, 2019, **627**.
9. C. Bannwarth, S. Ehlert and S. Grimme, *J. Chem. Theory Comput.*, 2019, **15**, 1652-1671.
10. M. J. Abraham, T. Murtola, R. Schulz, S. Páll, J. C. Smith, B. Hess and E. Lindahl, *SoftwareX*, 2015, **1-2**, 19-25.
11. J. Wang, R. M. Wolf, J. W. Caldwell, P. A. Kollman and D. A. Case, *J. Comput. Chem.*, 2004, **25**, 1157-1174.
12. M. Schauperl, P. S. Nerenberg, H. Jang, L.-P. Wang, C. I. Bayly, D. L. Mobley and M. K. Gilson, *Commun. Chem.*, 2020, **3**, 44.
13. T. Lu and F. Chen, *J. Comput. Chem.*, 2012, **33**, 580-592.
14. T. Lu, *J. Chem. Phys.*, 2024, **161**, 082503.
15. F. Neese, *WIREs Comput. Mol. Sci.*, 2022, **12**, e1606.
16. P. J. Stephens, F. J. Devlin, C. F. Chabalowski and M. J. Frisch, *J. Phys. Chem.*, 1994, **98**, 11623-11627.
17. F. Weigend and R. Ahlrichs, *PCCP*, 2005, **7**, 3297-3305.
18. T. Lu, Sobtop, Version 1.0(dev5). http://sobereva.com/soft/Sobtop (accessed 2026-02-27).
19. L. Martínez, R. Andrade, E. G. Birgin and J. M. Martínez, *J. Comput. Chem.*, 2009, **30**, 2157-2164.
20. G. Bussi, D. Donadio and M. Parrinello, *J. Chem. Phys.*, 2007, **126**, 014101.
21. M. Bernetti and G. Bussi, *J. Chem. Phys.*, 2020, **153**, 114107.
22. T. Darden, D. York and L. Pedersen, *J. Chem. Phys.*, 1993, **98**, 10089-10092.
23. B. Hess, H. Bekker, H. J. C. Berendsen and J. G. E. M. Fraaije, *J. Comput. Chem.*, 1997, **18**, 1463-1472.